

The Bethe-Salpeter equation at the critical end-point of the Mott transition

Erik G. C. P. van Loon^{1,2,*} and Friedrich Krien³

¹*Institut für Theoretische Physik, Universität Bremen, Otto-Hahn-Allee 1, 28359 Bremen, Germany*

²*Bremen Center for Computational Materials Science, Universität Bremen, Am Fallturm 1a, 28359 Bremen, Germany*

³*Jožef Stefan Institute, Jamova 39, SI-1000, Ljubljana, Slovenia*

Strong repulsive interactions between electrons can lead to a Mott metal-insulator transition. The Dynamical Mean-Field Theory (DMFT) explains the critical end-point and hysteresis region with single-particle concepts such as the spectral function and the quasiparticle weight. In this work, we reconsider the critical end point of the metal-insulator transition on the two-particle level. A divergence of the Bethe-Salpeter equation necessarily occurs at the critical point and simultaneously explains the thermodynamics of the hysteresis region and the iterative stability of the DMFT equations. In this way, the relevant eigenvalue and eigenvector of the Bethe-Salpeter equation provide a unified picture of the hysteresis region and of the critical end point of the Mott transition. This analysis paves the way for a deeper understanding of phase transitions in correlated materials.

The interplay of interactions, correlations and quantum statistics in quantum many-body physics is responsible for the appearance of complicated new phases, with the Mott transition [1] as a prominent example. The simplest theoretical realization of this correlation driven metal-insulator transition occurs in the (single-band) Hubbard model [2–5]. Quantum simulators using ultracold fermions in optical lattices are providing unprecedented experimental insight into this transition [6–10].

From the theory side, the Dynamical Mean-Field theory [11, 12] (DMFT) provides a rare example of an exact solution to a strongly correlated problem, namely to the Hubbard model in the limit of infinite dimensions. During the first decade after DMFT’s invention, the essence [13] of the Mott transition was ascertained [14–

21]: At the zero temperature transition to the insulating phase, the quasiparticle weight vanishes and the self-energy is divergent at small frequency, in contrast to the Fermi liquid. The U - T (interaction-temperature) DMFT phase diagram of the particle-hole symmetric model can be summarized as follows (sketched in Fig. 1, for an overview see Refs. [21–24]): at low temperature, there is a metallic phase at small $U < U_{c1}$ and an insulating phase at large $U > U_{c2}$. In between, for $U_{c1} < U < U_{c2}$, both metallic and insulating solutions can be stabilized. This hysteresis region (shaded blue area) ends at a critical temperature T_c , where $U_{c1} = U_{c2} = U_c$ (purple dot). No phase separation occurs in the particle-hole symmetric system [22].

Although the single-particle properties (Green’s function, self-energy, quasiparticle weight) are sufficient to understand the essentials of the metal-insulator transition, two-particle properties provide another rich layer of information about the response to external fields, spatial correlations, and optical properties. The simplifications of infinite dimensions allowed early studies at the two-particle level [17, 18, 25–28], but a systematic investigation of the DMFT two-particle physics had to wait [29–35] for computational improvement, especially the invention of continuous-time Quantum Monte Carlo solvers [36–38].

There has recently been a flurry of activity on divergences on the two-particle level [39–42], from simple toy models [43, 44] and the Hubbard atom [45] to cluster approaches [46], relating these divergences to unphysical solutions [40, 42, 47] and to the suppression of fluctuations [48], but without a clear link to the Mott transition. On the other hand, previous work [49] has established that the zero temperature critical point features a divergence of a two-particle quantity, namely the charge forward scattering amplitude.

Here we show that the two-particle level provides an intriguing new view on the Mott transition across the hys-

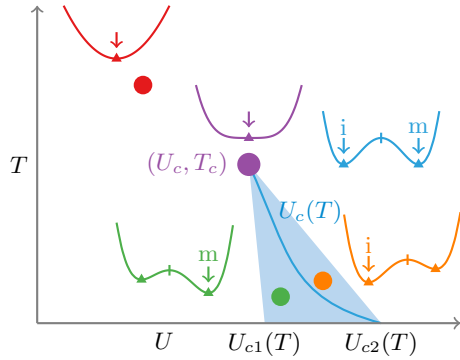


FIG. 1. Sketch of the phase diagram of the particle-hole symmetric Hubbard model in DMFT. The first-order metal-insulator transition occurs at $U_c(T)$ (blue curve), with a second-order critical end-point at (U_c, T_c) (purple dot). The shaded area is the hysteresis region, where both metal (m) and insulator (i) can be stabilized. The colored curves illustrate the free energy landscape at selected points (dots) in the phase diagram, the vertical marks denote the local maxima of the free energy, the triangles the local minima and the arrows the global minimum.

teresis region and especially at the critical end point, because the Bethe-Salpeter equation plays a double role in DMFT: It captures the response to external fields and to variations in the solution of the self-consistent equations. In particular, the Bethe-Salpeter kernel is *equivalent* to the Jacobian of the DMFT fixed point function, which determines the stability of iterative solutions [21, 23, 50]. The Bethe-Salpeter kernel is also directly related to the quadratic term in Landau’s free energy. This implies a divergence of the Bethe-Salpeter equation at the finite temperature critical end point of the metal-insulator hysteresis region. At particle-hole symmetry, the frequency structure of the corresponding eigenvector ensures that the compressibility stays finite, as discussed in more detail by Reitner et al. [51]. Therefore, the Bethe-Salpeter kernel determines two apparently separate stability criteria, the two-particle response and the iterative stability, and the eigenvector frequency structure – given by the difference between insulating and metallic solution – distinguishes between diverging response and exact cancellation.

We consider the Hubbard model describing the competition between localization due to the Coulomb interaction U and delocalization due to the dispersion t . We use i to label the sites on the periodic lattice and \mathbf{k} to label the corresponding momentum. The model is given by the Hamiltonian

$$H = - \sum_{\mathbf{k}, \sigma} t_{\mathbf{k}} c_{\mathbf{k}\sigma}^{\dagger} c_{\mathbf{k}\sigma} + U \sum_i n_{i\uparrow} n_{i\downarrow}, \quad (1)$$

where $c_{\mathbf{k}\sigma}^{\dagger}$ is the creation operator for a fermion with momentum \mathbf{k} and spin $\sigma = \uparrow, \downarrow$ and $n_{i\sigma} = c_{i\sigma}^{\dagger} c_{i\sigma}$ is the number operator of electrons with spin σ on site i . We consider this model in the grand-canonical ensemble at temperature T and chemical potential μ . A central object of interest is the (one-particle) Green’s function $G_{\mathbf{k}, \nu, \sigma} = - \langle c_{\sigma} c_{\sigma}^{\dagger} \rangle_{\mathbf{k}, \nu}$ in the Matsubara formalism, where $\nu_n = \pi T(2n + 1)$, with $n \in \mathbb{Z}$ the fermionic Matsubara frequencies. For compactness, we assume paramagnetism and drop the spin labels, derivations with all spin labels can be found in the supplemental material. Dyson’s equation relates G to the non-interacting ($U = 0$) Green’s function G_0 , as $G_{\mathbf{k}, \nu}^{-1} = (G_0)_{\mathbf{k}, \nu}^{-1} - \Sigma_{\mathbf{k}, \nu}$, thereby defining the self-energy Σ .

The Dynamical Mean-Field Theory [11, 12] (DMFT) provides an approximate solution to this model by setting $\Sigma_{\mathbf{k}, \nu} = \Sigma_{\nu}^{\text{AIM}}$, where AIM stands for an auxiliary impurity model consisting of a single interacting site in a self-consistently determined bath. For the present discussion, it is sufficient to state that the auxiliary impurity model serves as a tool to evaluate the functional relation $\Sigma[g]$ between the Green’s function g and the self-energy Σ of the AIM (in practice, we use the ALPS [52] CTQMC [38] solver of Ref. [53] with improved estimators [54]). This auxiliary impurity model is defined by

the self-consistency equation

$$g_{\nu} = \sum_{\mathbf{k}} G_{\mathbf{k}, \nu}[g] = \sum_{\mathbf{k}} \frac{1}{(G_0)_{\mathbf{k}, \nu}^{-1} - \Sigma_{\nu}[g]} \equiv f[g], \quad (2)$$

where from now on $\sum_{\mathbf{k}} \equiv \frac{1}{N} \sum_{\mathbf{k} \in \text{BZ}}$ denotes the momentum average over the Brillouin Zone. The square brackets denote functional relations, i.e., Σ_{ν} depends on $g_{\nu'}$, even when $\nu \neq \nu'$.

In this work, we consider the two-dimensional square lattice Hubbard model, $t_{\mathbf{k}} = -2t(\cos k_x + \cos k_y)$ at half-filling. The energy scale is set by $4t = 1$. The half-filled model is particle-hole symmetric, which leads to $\text{Re } g_{\nu} = 0$ and $\text{Re } \Sigma_{\nu} = U/2$. In other words, only the imaginary parts of both quantities are of interest, which simplifies the analysis.

Fixed point equation: The auxiliary impurity model is a finite system that cannot undergo a (finite temperature) phase transition by itself. Instead, as in Weiss’ mean field theory of magnetism, it is the self-consistency condition that opens the possibility of a phase transition. Therefore, our analysis of the critical point starts with the self-consistency condition.

DMFT looks for solutions of Eq. (2), i.e., a fixed point $f[g^*] = g^*$. An iterative scheme, $g^{(n+1)} = f[g^{(n)}]$, can be used to search for a fixed point. An important question is if these iterations converge to the fixed point g^* if one starts the iteration close to g^* . In that case, the fixed point is called attractive. The textbook analysis, based on a linear expansion of f around the fixed point, shows that g^* is attractive if and only if all eigenvalues of the Jacobian $\mathcal{J}|_{g^*} = (\delta f / \delta g)|_{g^*}$ have magnitude smaller than 1. Any eigenvalue larger than 1 implies that the self-consistency cycle is repulsive along the direction given by the corresponding eigenvector. For DMFT, the Jacobian can be evaluated explicitly in Matsubara space by using that $f[g]$ depends on g only via Σ ,

$$\begin{aligned} \mathcal{J}_{\nu\nu'} &= \sum_{\mathbf{k}} \frac{\delta G_{\mathbf{k}, \nu}}{\delta g_{\nu'}} = - \sum_{\mathbf{k}} G_{\mathbf{k}, \nu}^2 \frac{\delta G_{\mathbf{k}, \nu}^{-1}}{\delta g_{\nu'}} \\ &= \sum_{\mathbf{k}} G_{\mathbf{k}, \nu}^2 \frac{\delta \Sigma_{\nu}}{\delta g_{\nu'}} = T \sum_{\mathbf{k}} G_{\mathbf{k}, \nu}^2 \Gamma_{\omega=0, \nu\nu'} \\ &\equiv - \hat{X}_{\mathbf{q}=0} \hat{\Gamma} \equiv \hat{\mathcal{B}}. \end{aligned} \quad (3)$$

The functional derivative $\delta \Sigma / \delta g$ is the irreducible vertex Γ (times T), which is real for particle-hole symmetric systems [30], and we have introduced the notation $(\hat{X}_{\mathbf{q}})_{\nu\nu'} = -T \delta_{\nu\nu'} \sum_{\mathbf{k}} G_{\mathbf{k}, \nu} G_{\mathbf{k}+\mathbf{q}, \nu}$ for the “bubble” of DMFT Green’s functions. The hat denotes a matrix in Matsubara space and, when possible, the matrix indices ν, ν' are dropped. The AIM fully determines $\hat{\Gamma}$, \hat{X} brings in the necessary lattice information. In the last line, we recognize $\hat{\mathcal{B}}$ —the Bethe-Salpeter kernel at $\mathbf{q} = 0$ and $\omega = 0$ — a quantity that usually occurs in the calculation of linear response functions [12].

Response functions: Indeed, the DMFT recipe provided above not only allows us to determine the one-particle Green's function G for a given set of parameters (U, μ, T) . On top of this, DMFT also describes how the system would (linearly) respond [12] to an external field with frequency ω and momentum \mathbf{q} . We restrict our analysis to time-independent fields, $\omega = 0$. The response function $\chi_{\mathbf{q}}$ is obtained from the Bethe-Salpeter equation (BSE), a geometric matrix equation in Matsubara space,

$$\hat{\chi}_{\mathbf{q}}^{\text{DMFT}} = \frac{\hat{1}}{\hat{1} + \hat{X}_{\mathbf{q}}\hat{\Gamma}} \hat{X}_{\mathbf{q}} \stackrel{\mathbf{q}=0}{=} \frac{\hat{1}}{\hat{1} - \hat{\mathcal{B}}} \hat{X}_{\mathbf{q}=0}. \quad (4)$$

Here, the fraction denotes matrix inversion in Matsubara space and the matrix $\hat{1} - \hat{\mathcal{B}}$ in Eq. (4) is invertible if all eigenvalues of $\hat{\mathcal{B}}$ are smaller than 1 in magnitude.

From this generalized susceptibility matrix, the physical response function is obtained as a sum over both fermionic frequencies. For example, the compressibility $dn/d\mu$ is obtained from the generalized susceptibility at $\mathbf{q} = 0$ (and, as before, $\omega = 0$),

$$\frac{dn}{d\mu} = T^2 \sum_{\nu\nu'} (\hat{\chi}_{\mathbf{q}=0}^{\text{DMFT}})_{\nu\nu'}. \quad (5)$$

The response in DMFT is thermodynamically consistent in the sense that this Bethe-Salpeter determination of $dn/d\mu$ gives the same result as changing μ explicitly and calculating the change in n [55].

Landau theory: Following Landau, the free energy functional is the essential ingredient for understanding stable and unstable phases and hysteresis close to the critical point. Characteristic free energy curves are sketched in Fig. 1. The second derivative of the free energy determines if the stationary point is a local minimum ($\delta^2 F > 0$, stable, denoted by triangles in Fig. 1) or a local maximum ($\delta^2 F < 0$, unstable, denoted by a vertical bar). The critical point is where a stable point turns unstable, in other words, $\delta^2 F = 0$ exactly at the critical point (purple curve in Fig. 1).

The Mott transition of DMFT has been studied using Landau theory [21, 56, 57]. Chitra and Kotliar [58] have shown a relation between the Bethe-Salpeter equation and the free energy functional. Here we rederive a similar equation using Potthoff's self-energy functional [59] approach to DMFT. When evaluated at one of the fixed points, this functional is equal to the grand potential and thereby it provides direct access to information about thermodynamic stability [60].

The stationary point of the self-energy functional occurs when the first derivative is zero, resulting in the Dyson equation [59],

$$\frac{1}{T} \frac{\delta\Omega[\Sigma]}{\delta\Sigma} = \frac{1}{G_0^{-1} - \Sigma} - G = 0.$$

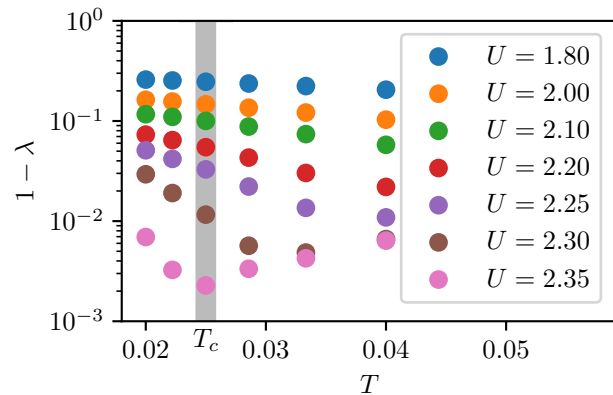


FIG. 2. The leading eigenvalue approaches unity close to the critical point (note the logarithmic scale). The vertical gray line shows the value of T_c extracted from Refs. 24 and 61.

To determine the stability of this solution, we proceed with the second derivative (Hessian),

$$\frac{1}{T} \frac{\delta^2\Omega}{\delta\Sigma^2} = \left(\frac{1}{G_0^{-1} - \Sigma} \right)^2 - \frac{\delta G}{\delta\Sigma} = G^2 - \left(\frac{\delta\Sigma}{\delta G} \right)^{-1}, \quad (6)$$

$$\left(\frac{\delta^2\Omega}{\delta(i\Sigma)^2} \right)^{-1} = \hat{\Gamma} \frac{\hat{1}}{\hat{1} - \hat{\mathcal{B}}},$$

where the stationary point (Dyson) equation was used.

Equation (6) is a matrix equation in Matsubara space, $\delta^2\Omega/\delta(i\Sigma)^2$ is the Hessian matrix, which is a real matrix in the case of particle-hole symmetry, and stability requires that all eigenvalues of the Hessian are positive. At the critical point, the Hessian changes from stable to unstable, i.e., one eigenvalue of $\delta^2\Omega/\delta\Sigma^2$ is equal to zero, so Eq. (6) needs to have a divergent eigenvalue.

The same Bethe-Salpeter kernel $\hat{\mathcal{B}}$ has appeared three times in stability criteria: in the Jacobian of the fixed point equation; in the compressibility; and in the second derivative of the self-energy functional. The latter two relate to the *stability* of the physical solution, whereas the Jacobian determines the *attractiveness* of the fixed point in an iterative scheme. For DMFT, these two aspects are tied together by the *same* Bethe-Salpeter kernel $\hat{\mathcal{B}}$.

This allows us to create a unified picture of the hysteresis region of the particle-hole symmetric metal-insulator transition. At the critical end point (U_c, T_c) , the purple dot in Fig. 1, the two stable (triangles in Fig. 1) and the one unstable (vertical marks in Fig. 1) stationary points merge together. Therefore, the quadratic part of the free energy functional vanishes at this point (purple curve), which together with Eq. (6) means that the Bethe-Salpeter kernel $\hat{\mathcal{B}}$ has an eigenvector V with eigenvalue $\lambda \rightarrow 1$ (Fig. 2) exactly at the critical end point. Since $\hat{\mathcal{B}}$ is equal to the Jacobian of the fixed point equation, the stable and unstable solutions correspond to attractive and repulsive fixed points, respectively [23]. As shown in the Supplemental Material, at the critical point,

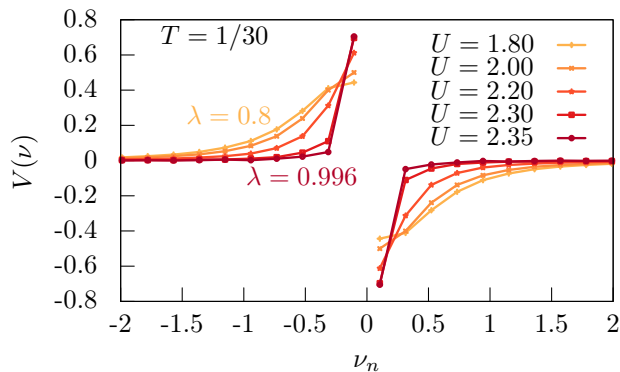


FIG. 3. The eigenvector V corresponding to the leading eigenvalue λ of the Bethe-Salpeter kernel, for T just above T_c . As U increases and the Mott transition is approached, the eigenvector localizes around $\nu = 0$ and $\lambda \rightarrow 1$. The eigenvector is normalized to $\sum_{\nu} |V(\nu)|^2 = 1$.

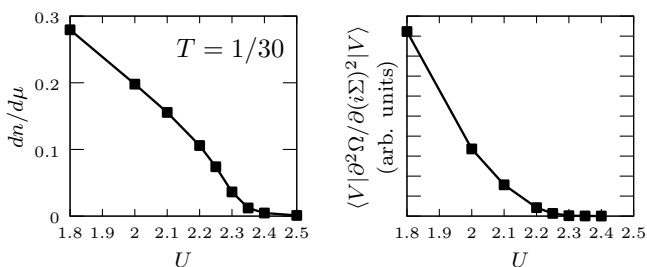


FIG. 4. Left: The compressibility stays finite as the Mott transition is approached. Right: The Hessian of the grand potential determines the thermodynamic stability. Along the direction of the leading BSE eigenvector V , $\langle V | \partial^2 \Omega / \partial (i\Sigma)^2 | V \rangle \rightarrow 0$ as the Mott transition is approached. The corresponding eigenvector V is shown in Fig. 3 as a function of U .

V is a simultaneous eigenvector of $\hat{\Gamma}$ and \hat{X} .

Figure 3 shows the eigenvector V close to the critical end point. The physical meaning of this eigenvector is that it relates the three fixed points that exist at $T < T_c$, as $g_m(\nu) - g_u(\nu) \propto (T_c - T)^\beta V(\nu)$ and $g_i(\nu) - g_u(\nu) \propto (T_c - T)^\beta V(\nu)$, where g_m , g_i and g_u are Green's function at the metallic, insulating and unstable fixed points, respectively, and β is a critical exponent. This together with particle-hole symmetry ($g(\nu) = -g(-\nu)$) implies $V(\nu) = -V(-\nu)$, i.e., the eigenvector V is antisymmetric [48]. As the difference between solutions, V provides the “order parameter” – similar to Kotliar's [56] $\delta\Delta_L$ at $T = 0$ – in the sense of Landau's functional: At the critical point, the free energy landscape goes from a parabola to a double well potential along the direction given by V . Figure 4 shows that the second derivative of the grand potential indeed vanishes as one gets close to the Mott transition.

The frequency structure of V , in Fig. 3, shows that

the three solutions $g(\nu)$ differ only at low frequency, i.e., close to the Fermi level. This is in agreement with what is known qualitatively from investigations of the Density of States: the difference between the insulator and the metal is that the latter has a quasiparticle peak at the Fermi level. Astretsov et al. [62] used a single Matsubara frequency approximation to study the cuprates, our result here is a direct quantitative proof that this kind of approximation is justified at the critical end point of the Mott transition.

At $T < T_c$ and $U_{c1} < U < U_{c2}$, the Bethe-Salpeter equation is convergent (and the iterative scheme is attractive) at both the metallic and the insulating solutions, $\lambda < 1$, and divergent (repulsive) at the unstable fixed point, $\lambda > 1$. Although both metallic and insulating solution are attractive fixed points, only one of them is the global minimum (c.f., green and orange curves in Fig. 1) of the free energy in most of the hysteresis region. Only at $U_c(T)$ (the blue line in Fig. 1), both solutions have exactly the same free energy, this is where the phase transition occurs. At U_{c1} (U_{c2}) the unstable and insulating (metallic) fixed point merge, so that $\lambda = 1$ at this fixed point, but the metallic (insulating) solution, with $\lambda < 1$, is the global minimum of the free energy.

Kotliar et al. [63] predicted a compressibility divergence at the critical end point of the doping-driven Mott transition, $dn/d\mu \rightarrow \infty$. On first sight, our present eigenvalue analysis seems to imply the same here, since the BSE diverges. However, a divergence in the BSE can be canceled by an exact orthogonality [48, 63], and that is indeed what happens at particle-hole symmetry [51]. The eigenvector $V \propto g_m - g_i$ is antisymmetric in ν and therefore does not contribute to the sum in Eq. (5) [48, 51, 64], so that $dn/d\mu$, shown in Fig. 4, is finite (and small) at the critical end point. This is consistent with the absence of phase separation at particle-hole symmetry [22]. A finite compressibility combined with a divergence of the BSE is reminiscent of the zero temperature case where, in fact, the divergence of the BSE is required so $dn/d\mu$ can vanish at the Mott transition [49]. In other words, both critical end points of the particle-hole symmetric Mott transition are characterized by a divergent BSE without a divergence in $dn/d\mu$.

The situation away from particle-hole symmetry is more complicated because of the complex-valuedness of the Green's functions [51]. The antiferromagnetic transition in DMFT [14] – which occurs when the assumption of paramagnetism is lifted – can also be analyzed along the lines of the current work as a divergence of the BSE in the magnetic channel. An important open question is the generalization of our analysis to the instabilities found in multi-orbital Hund's physics [65–72], and more generally to systems that show phase separation [22, 63, 73–81].

In conclusion, we identified the Bethe-Salpeter kernel with the Jacobian of the DMFT fixed point equation and with the curvature of the free energy functional. Near the

critical end point of the finite temperature correlation-driven Mott transition the BSE diverges. The eigenvector corresponding to the divergence relates the insulating and metallic solutions that exist below the critical temperature. Particle-hole symmetry then implies that this eigenvector is antisymmetric and does not contribute to the compressibility [51], which remains finite.

The authors thank M. Capone, P. Chalupa, H. Hafermann, M. Katsnelson, A. Lichtenstein, M. Schüler, A. Toschi, A. Valli and T. Wehling for stimulating discussions. E.G.C.P.v.L. is supported by the Zentrale Forschungsförderung of the Universität Bremen. F.K. acknowledges financial support from the Slovenian Research Agency under project number N1-0088.

* evloon@itp.uni-bremen.de

- [1] M. Imada, A. Fujimori, and Y. Tokura, Metal-insulator transitions, *Rev. Mod. Phys.* **70**, 1039 (1998).
- [2] J. Hubbard, Electron correlations in narrow energy bands, *Proc. R. Soc. A.* **276**, 238 (1963).
- [3] J. Kanamori, Electron correlation and ferromagnetism of transition metals, *Prog. Theor. Phys.* **30**, 275 (1963).
- [4] M. C. Gutzwiller, Effect of correlation on the ferromagnetism of transition metals, *Phys. Rev. Lett.* **10**, 159 (1963).
- [5] J. Hubbard, Electron correlations in narrow energy bands. III. an improved solution, *Proc. R. Soc. A.* **281**, 401 (1964).
- [6] R. Jördens, N. Strohmaier, K. Günter, H. Moritz, and T. Esslinger, A Mott insulator of fermionic atoms in an optical lattice, *Nature* **455**, 204 (2008).
- [7] U. Schneider, L. Hackermüller, S. Will, T. Best, I. Bloch, T. A. Costi, R. W. Helmes, D. Rasch, and A. Rosch, Metallic and insulating phases of repulsively interacting fermions in a 3d optical lattice, *Science* **322**, 1520 (2008).
- [8] R. Jördens, L. Tarruell, D. Greif, T. Uehlinger, N. Strohmaier, H. Moritz, T. Esslinger, L. De Leo, C. Kollath, A. Georges, V. Scarola, L. Pollet, E. Burovski, E. Kozik, and M. Troyer, Quantitative determination of temperature in the approach to magnetic order of ultracold fermions in an optical lattice, *Phys. Rev. Lett.* **104**, 180401 (2010).
- [9] P. M. Duarte, R. A. Hart, T.-L. Yang, X. Liu, T. Paiva, E. Khatami, R. T. Scalettar, N. Trivedi, and R. G. Hulet, Compressibility of a fermionic mott insulator of ultracold atoms, *Phys. Rev. Lett.* **114**, 070403 (2015).
- [10] D. Greif, M. F. Parsons, A. Mazurenko, C. S. Chiu, S. Blatt, F. Huber, G. Ji, and M. Greiner, Site-resolved imaging of a fermionic mott insulator, *Science* **351**, 953 (2016).
- [11] W. Metzner and D. Vollhardt, Correlated lattice fermions in $d = \infty$ dimensions, *Phys. Rev. Lett.* **62**, 324 (1989).
- [12] A. Georges, G. Kotliar, W. Krauth, and M. J. Rozenberg, Dynamical mean-field theory of strongly correlated fermion systems and the limit of infinite dimensions, *Rev. Mod. Phys.* **68**, 13 (1996).
- [13] New perspectives still appear, such as topological views on the transtion [82, 83].
- [14] M. Jarrell, Hubbard model in infinite dimensions: A quantum monte carlo study, *Phys. Rev. Lett.* **69**, 168 (1992).
- [15] A. Georges and W. Krauth, Numerical solution of the $d=\infty$ Hubbard model: Evidence for a Mott transition, *Phys. Rev. Lett.* **69**, 1240 (1992).
- [16] A. Georges and W. Krauth, Physical properties of the half-filled Hubbard model in infinite dimensions, *Phys. Rev. B* **48**, 7167 (1993).
- [17] X. Y. Zhang, M. J. Rozenberg, and G. Kotliar, Mott transition in the $d=\infty$ hubbard model at zero temperature, *Phys. Rev. Lett.* **70**, 1666 (1993).
- [18] M. J. Rozenberg, G. Kotliar, and X. Y. Zhang, Mott-Hubbard transition in infinite dimensions. II, *Phys. Rev. B* **49**, 10181 (1994).
- [19] R. M. Noack and F. Gebhard, Mott-hubbard transition in infinite dimensions, *Phys. Rev. Lett.* **82**, 1915 (1999).
- [20] R. Bulla, Zero temperature metal-insulator transition in the infinite-dimensional Hubbard model, *Phys. Rev. Lett.* **83**, 136 (1999).
- [21] N. Blümer, *Mott-Hubbard Metal-Insulator Transition and Optical Conductivity in High Dimensions*, Ph.D. thesis, University of Augsburg (2002).
- [22] M. Eckstein, M. Kollar, M. Potthoff, and D. Vollhardt, Phase separation in the particle-hole asymmetric Hubbard model, *Phys. Rev. B* **75**, 125103 (2007).
- [23] H. U. R. Strand, A. Sabashvili, M. Granath, B. Hellsing, and S. Östlund, Dynamical mean field theory phase-space extension and critical properties of the finite temperature Mott transition, *Phys. Rev. B* **83**, 205136 (2011).
- [24] T. Schäfer, F. Geles, D. Rost, G. Rohringer, E. Arrigoni, K. Held, N. Blümer, M. Aichhorn, and A. Toschi, Fate of the false Mott-Hubbard transition in two dimensions, *Phys. Rev. B* **91**, 125109 (2015).
- [25] A. Khurana, Electrical conductivity in the infinite-dimensional Hubbard model, *Phys. Rev. Lett.* **64**, 1990 (1990).
- [26] V. Zlatić and B. Horvatic, The local approximation for correlated systems on high dimensional lattices, *Solid State Communications* **75**, 263 (1990).
- [27] T. Pruschke, D. L. Cox, and M. Jarrell, Hubbard model at infinite dimensions: Thermodynamic and transport properties, *Phys. Rev. B* **47**, 3553 (1993).
- [28] M. J. Rozenberg, G. Kotliar, H. Kajueter, G. A. Thomas, D. H. Rapkine, J. M. Honig, and P. Metcalf, Optical conductivity in Mott-Hubbard systems, *Phys. Rev. Lett.* **75**, 105 (1995).
- [29] S. Brener, H. Hafermann, A. N. Rubtsov, M. I. Katsnelson, and A. I. Lichtenstein, Dual fermion approach to susceptibility of correlated lattice fermions, *Phys. Rev. B* **77**, 195105 (2008).
- [30] G. Rohringer, A. Valli, and A. Toschi, Local electronic correlation at the two-particle level, *Phys. Rev. B* **86**, 125114 (2012).
- [31] L. Boehnke and F. Lechermann, Competing orders in Na_xCoO_2 from strong correlations on a two-particle level, *Phys. Rev. B* **85**, 115128 (2012).
- [32] E. G. C. P. van Loon, H. Hafermann, A. I. Lichtenstein, A. N. Rubtsov, and M. I. Katsnelson, Plasmons in strongly correlated systems: Spectral weight transfer and renormalized dispersion, *Phys. Rev. Lett.* **113**, 246407 (2014).
- [33] D. Geffroy, J. Kaufmann, A. Hariki, P. Gunacker,

- A. Hausoel, and J. Kuneš, Collective modes in excitonic magnets: Dynamical mean-field study, *Phys. Rev. Lett.* **122**, 127601 (2019).
- [34] H. U. R. Strand, M. Zingl, N. Wentzell, O. Parcollet, and A. Georges, Magnetic response of Sr_2RuO_4 : Quasi-local spin fluctuations due to Hund's coupling, *Phys. Rev. B* **100**, 125120 (2019).
- [35] C. Melnick and G. Kotliar, Fermi liquid theory and divergences of the two-particle irreducible vertex in the periodic anderson lattice, arXiv e-prints (2020), [arXiv:2002.12904 \[cond-mat.str-el\]](https://arxiv.org/abs/2002.12904).
- [36] A. N. Rubtsov, V. V. Savkin, and A. I. Lichtenstein, Continuous-time quantum Monte Carlo method for fermions, *Phys. Rev. B* **72**, 035122 (2005).
- [37] P. Werner, A. Comanac, L. de' Medici, M. Troyer, and A. J. Millis, Continuous-time solver for quantum impurity models, *Phys. Rev. Lett.* **97**, 076405 (2006).
- [38] E. Gull, A. J. Millis, A. I. Lichtenstein, A. N. Rubtsov, M. Troyer, and P. Werner, Continuous-time Monte Carlo methods for quantum impurity models, *Rev. Mod. Phys.* **83**, 349 (2011).
- [39] T. Schäfer, G. Rohringer, O. Gunnarsson, S. Ciuchi, G. Sangiovanni, and A. Toschi, Divergent precursors of the Mott-Hubbard transition at the two-particle level, *Phys. Rev. Lett.* **110**, 246405 (2013).
- [40] E. Kozik, M. Ferrero, and A. Georges, Nonexistence of the Luttinger-Ward functional and misleading convergence of skeleton diagrammatic series for Hubbard-like models, *Phys. Rev. Lett.* **114**, 156402 (2015).
- [41] T. Schäfer, S. Ciuchi, M. Wallerberger, P. Thunström, O. Gunnarsson, G. Sangiovanni, G. Rohringer, and A. Toschi, Nonperturbative landscape of the Mott-Hubbard transition: Multiple divergence lines around the critical endpoint, *Phys. Rev. B* **94**, 235108 (2016).
- [42] O. Gunnarsson, G. Rohringer, T. Schäfer, G. Sangiovanni, and A. Toschi, Breakdown of traditional many-body theories for correlated electrons, *Phys. Rev. Lett.* **119**, 056402 (2017).
- [43] A. Stan, P. Romaniello, S. Rigamonti, L. Reining, and J. A. Berger, Unphysical and physical solutions in many-body theories: from weak to strong correlation, *New Journal of Physics* **17**, 093045 (2015).
- [44] R. Rossi and F. Werner, Skeleton series and multivaluedness of the self-energy functional in zero space-time dimensions, *Journal of Physics A: Mathematical and Theoretical* **48**, 485202 (2015).
- [45] P. Thunström, O. Gunnarsson, S. Ciuchi, and G. Rohringer, Analytical investigation of singularities in two-particle irreducible vertex functions of the Hubbard atom, *Phys. Rev. B* **98**, 235107 (2018).
- [46] J. Vučićević, N. Wentzell, M. Ferrero, and O. Parcollet, Practical consequences of the Luttinger-Ward functional multivaluedness for cluster DMFT methods, *Phys. Rev. B* **97**, 125141 (2018).
- [47] W. Tarantino, P. Romaniello, J. A. Berger, and L. Reining, Self-consistent dyson equation and self-energy functionals: An analysis and illustration on the example of the Hubbard atom, *Phys. Rev. B* **96**, 045124 (2017).
- [48] D. Springer, P. Chalupa, S. Ciuchi, G. Sangiovanni, and A. Toschi, Interplay between local response and vertex divergences in many-fermion systems with on-site attraction (2019), [arXiv:1912.02546 \[cond-mat.str-el\]](https://arxiv.org/abs/1912.02546).
- [49] F. Krien, E. G. C. P. van Loon, M. I. Katsnelson, A. I. Lichtenstein, and M. Capone, Two-particle Fermi liquid parameters at the Mott transition: Vertex divergences, Landau parameters, and incoherent response in dynamical mean-field theory, *Phys. Rev. B* **99**, 245128 (2019).
- [50] R. Žitko, Convergence acceleration and stabilization of dynamical mean-field theory calculations, *Phys. Rev. B* **80**, 125125 (2009).
- [51] M. Reitner, P. Chalupa, L. Del Re, D. Springer, S. Ciuchi, G. Sangiovanni, and A. Toschi, Attractive effect of a strong electronic repulsion – the physics of vertex divergences, arXiv e-prints , [arXiv:2002.12869 \(2020\)](https://arxiv.org/abs/2002.12869), [arXiv:2002.12869 \[cond-mat.str-el\]](https://arxiv.org/abs/2002.12869).
- [52] B. Bauer, L. D. Carr, H. G. Evertz, A. Feiguin, J. Freire, S. Fuchs, L. Gamper, J. Gukelberger, E. Gull, S. Guertler, A. Hehn, R. Igarashi, S. V. Isakov, D. Koop, P. N. Ma, P. Mates, H. Matsuo, O. Parcollet, G. Pawłowski, J. D. Picon, L. Pollet, E. Santos, V. W. Scarola, U. Schollwck, C. Silva, B. Surer, S. Todo, S. Trebst, M. Troyer, M. L. Wall, P. Werner, and S. Wessel, The ALPS project release 2.0: open source software for strongly correlated systems, *Journal of Statistical Mechanics: Theory and Experiment* **2011**, P05001 (2011).
- [53] H. Hafermann, P. Werner, and E. Gull, Efficient implementation of the continuous-time hybridization expansion quantum impurity solver, *Computer Physics Communications* **184**, 1280 (2013).
- [54] H. Hafermann, K. R. Patton, and P. Werner, Improved estimators for the self-energy and vertex function in hybridization-expansion continuous-time quantum Monte Carlo simulations, *Phys. Rev. B* **85**, 205106 (2012).
- [55] E. G. C. P. van Loon, H. Hafermann, A. I. Lichtenstein, and M. I. Katsnelson, Thermodynamic consistency of the charge response in dynamical mean-field based approaches, *Phys. Rev. B* **92**, 085106 (2015).
- [56] G. Kotliar, Landau theory of the Mott transition in the fully frustrated Hubbard model in infinite dimensions, *The European Physical Journal B - Condensed Matter and Complex Systems* **11**, 27 (1999).
- [57] G. Kotliar, E. Lange, and M. J. Rozenberg, Landau theory of the finite temperature Mott transition, *Phys. Rev. Lett.* **84**, 5180 (2000).
- [58] R. Chitra and G. Kotliar, Effective-action approach to strongly correlated fermion systems, *Phys. Rev. B* **63**, 115110 (2001).
- [59] M. Potthoff, Self-energy-functional approach to systems of correlated electrons, *The European Physical Journal B - Condensed Matter and Complex Systems* **32**, 429 (2003).
- [60] M. Balzer, B. Kyung, D. Sénéchal, A.-M. S. Tremblay, and M. Potthoff, First-order Mott transition at zero temperature in two dimensions: Variational plaquette study, *EPL (Europhysics Letters)* **85**, 17002 (2009).
- [61] H. T. Dang, X. Y. Xu, K.-S. Chen, Z. Y. Meng, and S. Wessel, Mott transition in the triangular lattice Hubbard model: A dynamical cluster approximation study, *Phys. Rev. B* **91**, 155101 (2015).
- [62] G. V. Astretsov, G. Rohringer, and A. N. Rubtsov, Dual parquet scheme for the two-dimensional Hubbard model: Modeling low-energy physics of high- T_c cuprates with high momentum resolution, *Phys. Rev. B* **101**, 075109 (2020).
- [63] G. Kotliar, S. Murthy, and M. J. Rozenberg, Compressibility divergence and the finite temperature Mott transition, *Phys. Rev. Lett.* **89**, 046401 (2002).

- [64] P. Chalupa, P. Gunacker, T. Schäfer, K. Held, and A. Toschi, Divergences of the irreducible vertex functions in correlated metallic systems: Insights from the Anderson impurity model, *Phys. Rev. B* **97**, 245136 (2018).
- [65] P. Werner, E. Gull, M. Troyer, and A. J. Millis, Spin freezing transition and Non-Fermi-Liquid self-energy in a three-orbital model, *Phys. Rev. Lett.* **101**, 166405 (2008).
- [66] K. Haule and G. Kotliar, Coherence–incoherence crossover in the normal state of iron oxypnictides and importance of Hund’s rule coupling, *New Journal of Physics* **11**, 025021 (2009).
- [67] L. de’ Medici, S. R. Hassan, M. Capone, and X. Dai, Orbital-selective Mott transition out of band degeneracy lifting, *Phys. Rev. Lett.* **102**, 126401 (2009).
- [68] L. de’ Medici, J. Mravlje, and A. Georges, Janus-faced influence of Hund’s rule coupling in strongly correlated materials, *Phys. Rev. Lett.* **107**, 256401 (2011).
- [69] P. Werner, M. Casula, T. Miyake, F. Aryasetiawan, A. J. Millis, and S. Biermann, Satellites and large doping and temperature dependence of electronic properties in hole-doped BaFe₂As₂, *Nature Physics* **8**, 331 (2012).
- [70] K. M. Stadler, Z. P. Yin, J. von Delft, G. Kotliar, and A. Weichselbaum, Dynamical mean-field theory plus numerical renormalization-group study of spin-orbital separation in a three-band Hund metal, *Phys. Rev. Lett.* **115**, 136401 (2015).
- [71] L. de’ Medici, Hund’s induced Fermi-liquid instabilities and enhanced quasiparticle interactions, *Phys. Rev. Lett.* **118**, 167003 (2017).
- [72] P. Villar Arribi and L. de’ Medici, Hund-enhanced electronic compressibility in FeSe and its correlation with T_c , *Phys. Rev. Lett.* **121**, 197001 (2018).
- [73] M. Grilli, R. Raimondi, C. Castellani, C. Di Castro, and G. Kotliar, Superconductivity, phase separation, and charge-transfer instability in the $U = \infty$ limit of the three-band model of the CuO₂ planes, *Phys. Rev. Lett.* **67**, 259 (1991).
- [74] P. Majumdar and H. R. Krishnamurthy, Lattice contraction driven insulator-metal transition in the $d = \infty$ local approximation, *Phys. Rev. Lett.* **73**, 1525 (1994).
- [75] A. Tandon, Z. Wang, and G. Kotliar, Compressibility of the two-dimensional infinite- U Hubbard model, *Phys. Rev. Lett.* **83**, 2046 (1999).
- [76] K. Held, A. K. McMahan, and R. T. Scalettar, Cerium volume collapse: Results from the merger of dynamical mean-field theory and local density approximation, *Phys. Rev. Lett.* **87**, 276404 (2001).
- [77] M. Capone, G. Sangiovanni, C. Castellani, C. Di Castro, and M. Grilli, Phase separation close to the density-driven Mott transition in the Hubbard-Holstein model, *Phys. Rev. Lett.* **92**, 106401 (2004).
- [78] M. Aichhorn, E. Arrighoni, M. Potthoff, and W. Hanke, Phase separation and competition of superconductivity and magnetism in the two-dimensional Hubbard model: From strong to weak coupling, *Phys. Rev. B* **76**, 224509 (2007).
- [79] S. Lupi, L. Baldassarre, B. Mansart, A. Perucchi, A. Barinov, P. Dudin, E. Papalazarou, F. Rodolakis, J.-P. Rueff, J.-P. Itié, *et al.*, A microscopic view on the Mott transition in chromium-doped V₂O₃, *Nature communications* **1**, 105 (2010).
- [80] J. Otsuki, H. Hafermann, and A. I. Lichtenstein, Superconductivity, antiferromagnetism, and phase separation in the two-dimensional Hubbard model: A dual-fermion approach, *Phys. Rev. B* **90**, 235132 (2014).
- [81] C.-H. Yee and L. Balents, Phase separation in doped Mott insulators, *Phys. Rev. X* **5**, 021007 (2015).
- [82] D. E. Logan and M. R. Galpin, Mott insulators and the doping-induced Mott transition within DMFT: exact results for the one-band Hubbard model, *Journal of Physics: Condensed Matter* **28**, 025601 (2015).
- [83] S. Sen, P. J. Wong, and A. K. Mitchell, The Mott transition as a topological phase transition (2020), arXiv:2001.10526 [cond-mat.str-el].

SUPPLEMENTAL MATERIAL: SIGN CONVENTION AND DETAILED DERIVATIONS

The literature contains different definitions of the vertex, especially concerning the sign. Here, we take as the fundamental equation

$$\Gamma_{\nu\nu'}^{\sigma\sigma'} \equiv +\frac{1}{T} \frac{\delta\Sigma_{\nu\sigma}}{\delta g_{\nu'\sigma'}}. \quad (7)$$

It is instructive to apply this to the Hartree-Fock self-energy,

$$\Sigma_{\nu\sigma}^{\text{HF}} = UT \sum_{\nu',\sigma' \neq \sigma} g_{\nu,\sigma'}, \quad (8)$$

$$\Gamma_{\nu\nu'}^{\sigma\sigma'} = \frac{1}{T} \frac{\delta\Sigma_{\nu\sigma}}{\delta g_{\nu'\sigma'}} = U(1 - \delta_{\sigma\sigma'}), \quad (9)$$

$$\Gamma^{\uparrow\downarrow} = +U, \quad (10)$$

$$\Gamma^{\uparrow\uparrow} = 0, \quad (11)$$

$$\Gamma^{\text{sp}} \equiv \Gamma^{\uparrow\uparrow} - \Gamma^{\uparrow\downarrow} = -U, \quad (12)$$

$$\Gamma^{\text{ch}} \equiv \Gamma^{\uparrow\uparrow} + \Gamma^{\uparrow\downarrow} = +U. \quad (13)$$

In other words, $\Gamma > 0$ signals *repulsion* in that channel. We define the bubble X and generalized susceptibility χ so that both are positive, after being summed over Matsubara frequencies,

$$X_{\nu\nu',\sigma\sigma'} \equiv -T\delta_{\nu\nu'}\delta_{\sigma\sigma'} \sum_{\mathbf{k}} G_{\nu,\sigma,\mathbf{k}} G_{\nu',\sigma,\mathbf{k}}, \quad (14)$$

$$\hat{\chi}^{\text{DMFT}} \equiv \frac{\hat{1}}{\hat{1} + \hat{X}\hat{\Gamma}} \hat{X}. \quad (15)$$

Expanding the denominator to first order shows that if $U > 0$ ($\Gamma^{\text{ch}} > 0$), then $\chi < X$, a repulsive interaction suppresses the corresponding susceptibility. Our sign convention for Γ is opposite to Georges et al. [12], who use $\chi^{\text{DMFT}} = \hat{1}/(\hat{1} - \hat{X}\hat{\Gamma})\hat{X}$. Based on the denominator of the Bethe-Salpeter equation, we define the Bethe-Salpeter kernel $\hat{\mathcal{B}}$ as

$$\hat{\mathcal{B}} = -\hat{X}\hat{\Gamma}, \quad (16)$$

so that an eigenvalue of +1 corresponds to the divergence of the Bethe-Salpeter equation.

With spin and Matsubara labels, the Jacobian reads

$$\begin{aligned}
\mathcal{J}_{\nu\nu',\sigma\sigma'} &= \frac{\partial f_{\nu\sigma}}{\partial g_{\nu'\sigma'}} \quad (17) \\
&= \sum_{\mathbf{k}} \frac{\delta G_{\mathbf{k},\nu\sigma}}{\delta g_{\nu'\sigma'}} \\
&= - \sum_{\mathbf{k}} G_{\mathbf{k},\nu\sigma}^2 \frac{\delta G_{\mathbf{k},\nu\sigma}^{-1}}{\delta g_{\nu'\sigma'}} \\
&= + \sum_{\mathbf{k}} G_{\mathbf{k},\nu\sigma}^2 \frac{\delta \Sigma_{\nu\sigma}}{\delta g_{\nu'\sigma'}} \\
&= +T \sum_{\mathbf{k}} G_{\mathbf{k},\nu\sigma}^2 \Gamma_{\nu\nu'}^{\sigma\sigma'} \\
&= -\hat{X}_{\nu\nu',\sigma\sigma'} \hat{\Gamma}_{\nu\nu'}^{\sigma\sigma'} \\
&= \hat{\mathcal{B}}. \quad (18)
\end{aligned}$$

If we consider paramagnetic solutions, $g_\sigma = g_{\sigma'} = g$ change in the same way and we get

$$\frac{\partial f_{\nu,\uparrow}}{\partial g} = \frac{\partial f_{\nu,\uparrow}}{\partial g_\uparrow} + \frac{\partial f_{\nu,\uparrow}}{\partial g_\downarrow} = \mathcal{B}^{\uparrow\uparrow} + \mathcal{B}^{\uparrow\downarrow} = \mathcal{B}^{\text{ch}}, \quad (19)$$

i.e., for paramagnetic solutions only the charge channel of the Bethe-Salpeter kernel is relevant.

The second derivative of the free energy functional is

$$\begin{aligned}
\frac{1}{T} \frac{\delta^2 \Omega}{\delta \Sigma_{\nu\sigma} \delta \Sigma_{\nu'\sigma'}} &= \delta_{\nu\nu'} \delta_{\sigma\sigma'} \left(\frac{1}{(G_0^{-1})_{\nu\sigma} - \Sigma_{\nu\sigma}} \right)^2 - \frac{\delta G_{\nu'\sigma'}}{\delta \Sigma_{\nu\sigma}} \\
&= \delta_{\nu\nu'} \delta_{\sigma\sigma'} G_{\nu\sigma}^2 - \left(\frac{\delta \Sigma_{\nu\sigma}}{\delta G_{\nu'\sigma'}} \right)^{-1} \\
&= -\frac{1}{T} \left(\hat{X}_{\nu\nu',\sigma\sigma'} + \left(\hat{\Gamma}_{\nu\nu'}^{\sigma\sigma'} \right)^{-1} \right). \quad (20)
\end{aligned}$$

$$\left(\frac{\delta^2 \Omega}{\delta \Sigma_{\nu\sigma} \delta \Sigma_{\nu'\sigma'}} \right)^{-1} = -\hat{\Gamma} \frac{\hat{1}}{\hat{1} + \hat{X}\hat{\Gamma}} = -\hat{\Gamma} \frac{\hat{1}}{\hat{1} - \hat{\mathcal{B}}}. \quad (21)$$

As with the Jacobian, the restriction to paramagnetic solutions selects the charge channel of Γ and \mathcal{B} .

Although Σ is generally a complex function, at particle-hole symmetry Σ is purely imaginary (modulo the constant Hartree contribution), so it is sufficient to look at $\delta^2 \Omega / \delta (i\Sigma)^2$. On the right-hand side, $\hat{\Gamma}$ and \hat{X} are real matrices and therefore Ω is a real function. Because of this, it makes sense to talk about minima and maxima and not just about stationary points.

At the critical point, one eigenvalue of the Hessian $\delta^2 \Omega / \delta \Sigma^2$ changes sign, the corresponding eigenvector determines the unstable direction of the free energy landscape.

Formally, the self-energy functional and the grand potential only coincide at the stationary point(s). In a Landau theory analysis of the critical region, three stationary points are close together, with a free energy landscape

described by lowest-order polynomials (up to ϕ^4). Since the grand potential Φ and the functional Ω are equal at all stationary points, and the stationary points move arbitrarily close together as the critical end point is approached, local minima in the grand potential will correspond to local minima in Ω . Furthermore, the density is fixed at particle-hole symmetry, so the grand potential (given here by Ω) is equal to the free energy, modulo a constant shift.

In general, there is no reason for the Hessian and the Bethe-Salpeter kernel to have the same eigenbasis, since Eq. (21) is a matrix equation. However, it is easy to show that exactly at the critical point, the eigenvector V with $\hat{\mathcal{B}}V = V$ is also a left eigenvector of the Hessian with eigenvalue 0:

$$\langle V | \delta^2 \Omega / \delta \Sigma^2 = -\langle V | (\hat{1} - \hat{\mathcal{B}}) \hat{\Gamma}^{-1} = -\langle V | 0 \hat{\Gamma}^{-1} = \langle V | 0.$$

The Hessian is symmetric, so the left eigenvector V is also a right eigenvector of the Hessian. From $(\hat{1} - \hat{\mathcal{B}}) \hat{\Gamma}^{-1} |V\rangle = 0$, it then follows that $\hat{\Gamma}^{-1} |V\rangle$ is an eigenvector of $\hat{\mathcal{B}}$ with eigenvalue 1. Altogether, assuming that the eigenvalue 1 of \mathcal{B} is not degenerate, this shows that V is also an eigenvector of Γ^{-1} and thus also of \hat{X} and of any combination of Γ and \hat{X} . Since \hat{X} is Matsubara diagonal, with eigenvalues that only depend on $|\nu|$, this strongly suggests that the eigenvector V should be localized onto a single pair of frequencies at the critical point, as we indeed observe in Fig. 3. The only alternative would be an accidental degeneracy of eigenvalues of \hat{X} corresponding to different Matsubara frequencies.

The combination shown in Fig. 4,

$$\langle V | \frac{\delta^2 \Omega}{\delta (i\Sigma)^2} |V\rangle = (\lambda - 1) \langle V | \hat{\Gamma}^{-1} |V\rangle, \quad (22)$$

with V the leading Bethe-Salpeter eigenvector, approaches the relevant eigenvalue of the Hessian as one goes towards the critical point. Note that the eigenvector V is only determined up to a scale factor, the results shown in Fig. 4 use $\sum_{\nu} |V(\nu)|^2 = 1$, as in Fig. 3.

To summarize, the three central equations read,

$$\hat{\mathcal{J}} = \hat{\mathcal{B}}, \quad (23)$$

$$\hat{\chi} = \frac{\hat{1}}{\hat{1} - \hat{\mathcal{B}}} \hat{X}, \quad (24)$$

$$\left(\frac{\delta^2 \Omega}{\delta (i\Sigma)^2} \right)^{-1} = \hat{\Gamma} \frac{\hat{1}}{\hat{1} - \hat{\mathcal{B}}}. \quad (25)$$

The critical eigenvector V is a simultaneous eigenvector of all three matrices.